iScience

CellPress

Article

Pyrenetetrone Derivatives Tailored by Nitrogen Dopants for High-Potential Cathodes in Lithium-Ion Batteries

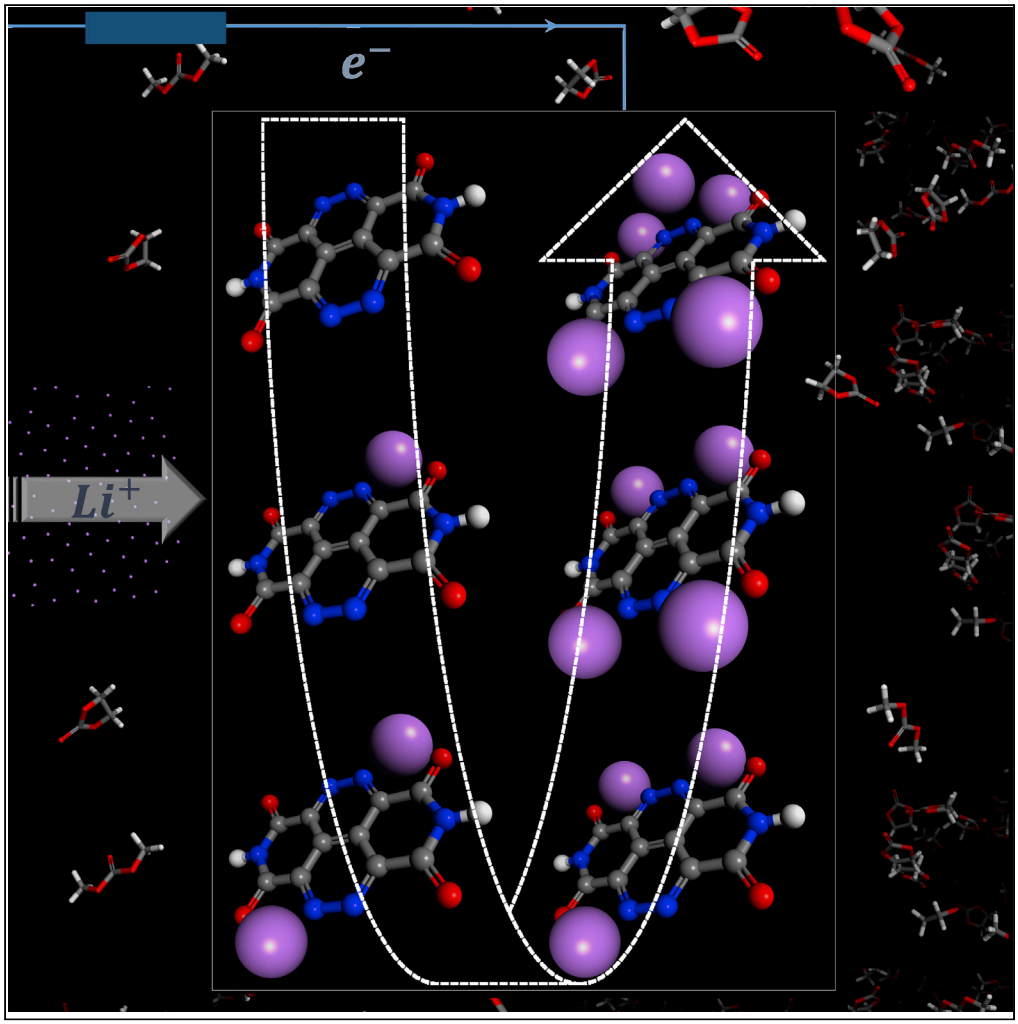

Chae Young Go, Gyeong Seok Jeong, Ki Chul Kim

kich2018@konkuk.ac.kr

HIGHLIGHTS

Redox property can be tailored by the systematic nitrogen doping process

Redox potential is perfectly correlated with electron affinity and solvation energy

Pyrenetetrones exhibit two-stage transition behaviors during the discharging process

Solvation energy plays a crucial role in the cathodic deactivation of pyrenetetrones

Go et al., iScience *21*, 206–216
November 22, 2019
https://doi.org/10.1016/j.isci.2019.10.023

iScience

CellPress

Article

Pyrenetetrone Derivatives Tailored by Nitrogen Dopants for High-Potential Cathodes in Lithium-Ion Batteries

Chae Young Go,[1] Gyeong Seok Jeong,[1] and Ki Chul Kim[1,2,*]

SUMMARY

To overcome limited information on organic cathode materials for lithium-ion batteries, we studied the electrochemical redox properties of pyrenetetrone and its nitrogen-doped derivatives. Three primary conclusions are highlighted from this study. First, the redox potential increases as the number of electron-withdrawing nitrogen dopants increases. Second, the redox potentials of pyrenetetrone derivatives continuously decrease with the number of bound Li atoms during the discharging process owing to the decrease in the reductive ability until the compounds become cathodically deactivated exhibiting negative redox potentials. Notably, pyrenetetrone with four nitrogen dopants loses its cathodic activity after the binding of five Li atoms, indicating remarkably high performance (496 mAh/g and 913 mWh/g). Last, the redox potential is strongly correlated not only with electronic properties but also with solvation energy. This highlights that pyrenetetrone derivatives would follow two-stage transition behaviors during the discharging process, implying a crucial contribution of solvation energy to their cathodic deactivation.

INTRODUCTION

Energy demand has increased with technological improvements since the industrial revolution, and accordingly the depletion of fossil fuels has come up as a challenging issue (Dincer, 2000). In addition, these fossil fuels have made a critical issue in the environmental aspect owing to their environmentally harmful nature (Dincer, 2000). Various alternative energy resources, such as solar energy, wind energy, and geothermal energy, have been therefore studied to resolve this energy problem (Solangi et al., 2011; Herbert et al., 2007; Lund and Boyd, 2016). However, the intermittent characteristics of technologies harvesting such renewable energies have led to the special attention to advanced energy storage technologies to stably supply the produced energy resources for a variety of applications (Gür, 2018; Chen et al., 2009). In particular, the increasing demand on portable electronic devices and electric vehicles has resulted in the tremendous interest in electrochemical energy storage devices (Gür, 2018; Chen et al., 2009). As one of promising rechargeable battery candidates, lithium-ion batteries are widely utilized for these applications owing to their high charge capacities and energy densities (Goodenough and Park, 2013; Nitta et al., 2015).

Delicate optimization of graphitic anodes, inorganic cathodes, organic electrolytes, and insulating separators has allowed us to have lithium-ion batteries with impressive performance in the electrochemical energy storage (Marom et al., 2011; Aurbach et al., 2004; Xiang et al., 2016). In particular, inorganic cathodes, such as transition metal oxides, phosphates, silicates, and sulfates, have been widely utilized to store a large amount of charge in their ordered lattices through electrochemical reactions (Goodenough and Park, 2013; Nitta et al., 2015). For instance, $LiCoO_2$ and $LiFePO_4$ cathode materials occupy the major cathode material position in commercial lithium-ion battery markets because they can provide the high energy densities and reasonable cyclic stabilities (Takahashi et al., 2008). However, the diffusion of Li ions in such inorganic materials is typically slow, resulting in the limited power densities, which would be the main challenge against the full commercialization (Goodenough and Park, 2013).

Owing to the facilitated ionic diffusion arising from the structural flexibility as well as the environmentally benign characteristics, facilitated fabrication process, and cost-effectiveness, organic materials have recently attracted a tremendous interest as alternative cathode materials to replace the conventional inorganic materials (Wu et al., 2017; Luo et al., 2018; Wang et al., 2013; Lee et al., 2010, 2011; Song et al., 2015a, 2015b; Nokami et al., 2012). An early-stage attention to carbon materials, such as graphenes, carbon

[1]Computational Materials Design Laboratory, Division of Chemical Engineering, Konkuk University, Seoul 05029, The Republic of Korea

[2]Lead Contact

*Correspondence: kich2018@konkuk.ac.kr

https://doi.org/10.1016/j.isci.2019.10.023

nanotubes, and their hybrid materials, has been extended toward a variety of small redox-active organic molecules including quinones, dopamines, vitamins, and graphene flakes. For example, Schon et al. developed bio-derived pendant polymer cathodes with the redox moiety of flavin, which was derived from riboflavin (vitamin B2) (Schon et al., 2016). Their investigation on the redox properties and cell performance of the biopolymer-derived cathodes resulted in a charge capacity of 125 mAh/g at 0.1 C and an operating potential of 2.5 V versus Li/Li^+. Liu et al. developed an organic cathode consisting of self-polymerized dopamine spontaneously coated on the surfaces of few-walled carbon nanotubes (FWNTs)(Liu et al., 2017). They demonstrated that multiple redox reactions between the self-polymerized dopamines and electrolyte ions in the high voltage region from 2.5 to 4.1 V versus Li/Li^+ as well as the double layer capacitance from FWNTs would result in gravimetric capacities of ~133 mAh/g in lithium-ion batteries and ~109 mAh/g in sodium-ion batteries. Kim et al. employed the first-principles density functional theory (DFT) modeling approach to investigate the Li-binding thermodynamics and redox properties of seven quinone derivatives as cathodes in lithium-ion batteries (Kim et al., 2016a, 2016b). They highlighted that the redox properties of the quinone derivatives would strongly rely on their structural and electronic properties exhibiting both the redox potential and charge capacity enhanced by the functionalization of electron-withdrawing carboxylic acids. Ma et al. studied the redox properties of a sulfur heterocyclic quinone (i.e., dibenzo[b,i]thianthrene-5,7,12,14-tetraone, namely, DTT) with a conductive polymer binder (Ma et al., 2016). They reported that the sulfur atoms in the DTT could be the main resource to exhibit the initial lithium intercalation potential of the DTT higher by 0.3 V than that of its carbon analog. Nokami et al. reported that pyrene-4,5,9,10-tetraone bound to polymethacrylate could show remarkable charge/discharge properties with a high charge capacity of 231 mAh/g and fast charge/discharge ability retaining its cyclic stability (Nokami et al., 2012). Despite their numerous promises, critical challenges remain to be resolved for practical applications: (1) the dissolution of small organic molecules by organic solvents, (2) poor electronic conductivity, (3) relatively low operating voltages for organic materials as compared with inorganic materials, and (4) relatively low charge capacities of organic materials as compared with their high-power densities. The former two bottlenecks might be resolved by introducing polymerization processes and incorporating conductive additives, whereas the latter two issues are still veiled to be explored (Nokami et al., 2012; Schon et al., 2016; Liu et al., 2017).

Herein, we explore a redox-active organic molecule, namely, pyrenetetrone, and its nitrogen-doped derivatives to evaluate their potential as cathodes in lithium-ion batteries. The first-principles DFT modeling approach is employed to investigate the cell performances as well as the electrochemical redox properties. We primarily focus on the discussion of the following issues: the correlations of the redox properties of the molecules with (1) the structural properties, (2) electronic properties, and (3) Li-involved discharging process.

RESULTS

The core parameter employed in this study is the redox potential calculated by the first-principles DFT modeling approach. Previous studies have reported that the computational protocol could provide accurate redox potentials for a variety of organic compounds (Kim et al., 2016a, 2016b; Er et al., 2015). For example, Jang and coworkers explored the redox potentials for a series of quinone derivatives and highlighted that the protocol could predict the redox potentials with an uncertainty of ~0.3 V as compared with electrochemically measured values (Kim et al., 2016a, 2016b). Aspuru-Guzik and coworkers accurately calculated the redox potentials for a broad array of quinones (Er et al., 2015). Our preliminary calculations also verify that the computational protocol would reliably predict the redox potentials of organic molecules, as listed in Table 1. The highly accurate computational protocol would enable us to draw meaningful conclusions from a systematic analysis of the calculated redox potentials and theoretical performance parameters in the subsequent sections.

A computational approach utilizing the binding mechanisms of charge carriers (i.e., Li and Na) has been also utilized to predict cell voltages of secondary batteries (Meng and Dompablo, 2009; Ong et al., 2011). This approach usually requires unambiguously well-defined positions for the charge carriers bound to cathode materials to reliably predict the cell voltages. Hence, this protocol has been widely employed as a powerful tool to explore the redox properties of inorganic cathode materials (Meng and Dompablo, 2009; Ong et al., 2011). In contrast, this approach is not effective for organic cathode materials primarily due to two reasons: (1) the uncertainty in the position for Li atoms bound to organic materials and (2) the uncertainty in reliably predicting crystalline structures. Note that organic cathode materials experience the

Molecule	Redox Potential (V versus Li/Li^+)	
	DFT Method (This Work)	Experiment
1,4-Benzoquinone	2.9	3.1 (ref. 23)
1,4-Naphthoquinone	2.6	2.6 (ref. 23)
9,10-Anthraquinone	2.3	2.2 (ref. 23)
2-Aminoanthraquinone	2.1	2.1 (ref. 23)
2,6-Diaminoanthraquinone	1.9	2.0 (ref. 23)
Anthraquinone-2-carboxylic acid	2.4	2.3 (ref. 23)
1,4-Benzenedicarbonitrile	1.7	1.7 (ref. 42)
Pyrenetetrone	2.7	2.5 (ref. 43)
Thiophene	−0.2	−0.1 (ref. 43)
Furan	−0.8	−1.1 (ref. 43)
Benzopyrrole	−0.2	−0.2 (ref. 43)

Table 1. Validation of Our Computational Protocol

The redox potentials for a broad range of organic compounds predicted by both the first-principles DFT method (this work) and experimental measurements (Kim et al., 2016a, 2016b; Roth et al., 2016; Araujo et al., 2017).

electrochemical reduction process followed by the accommodation of the cathode materials with Li cations during the discharging process. Thus, our computational protocol estimating the intrinsic electrochemical reduction potentials for the organic cathode materials would be appropriate for the organic materials whose lithiated structures are not clearly informed.

Redox Properties and Performances

Seven pyrenetetrone derivatives (including the pristine pyrenetetrone) were modeled systematically by introducing structural and electronic variations in the basic molecule, pyrenetetrone, as shown in Figure 1. In the notation *m*N-*n*-pyrenetetrone, *m* and *n* indicate the number of nitrogen dopants and the case number, respectively. The case number is only applied to the three pyrenetetrone derivatives with two nitrogen dopants. For example, 2N-1-pyrenetetrone is a pyrenetetrone derivative in which two nitrogen dopants are placed in the nearest neighboring positions, whereas 4N-pyrenetetrone has four nitrogen dopants in its structure.

We investigated the redox potentials of the seven pyrenetetrone derivatives to fundamentally understand their redox properties in various aspects and assess their potential for cathodes in lithium-ion batteries. All detailed information on the redox potential is listed in Table S1. Specifically, the redox potential can be correlated with the structural properties, such as the number density and configuration of the incorporated nitrogen dopants, as shown in Figure 2. It is verified from the figure that the redox potentials for the bare molecules at fully charged states increase as the number of the nitrogen dopants increases, exhibiting the lowest and highest redox potentials for pyrenetetrone (2.67 V versus Li/Li^+) and 4N-pyrenetetrone (3.70 V versus Li/Li^+), respectively. It is expected that the inductive effect arising from the addition of the nitrogen dopants with electron-withdrawing nature would make the central backbone electron-deficient and reductive. In contrast, the redox potential is predicted to be insensitive to the relative position of nitrogen dopants, as shown for the three pyrenetetrone derivatives with two nitrogen dopants in Figure 2B. All the three bare molecules have the redox potentials ranged within 3.13–3.29 V versus Li/Li^+, indicating that the redox potential would be not affected by the geometric configurations of the nitrogen dopants under the condition of the fixed number of the dopants.

During the discharging process, Li binds to the bare pyrenetetrone derivatives sequentially as shown in Figure S1. To identify the most stable configurations of Li atoms binding to each bare pyrenetetrone derivative, we considered all possible Li-binding configurations and then examined their relative thermodynamic stability. Please note that Li atoms are assumed to be sequentially bound to the most

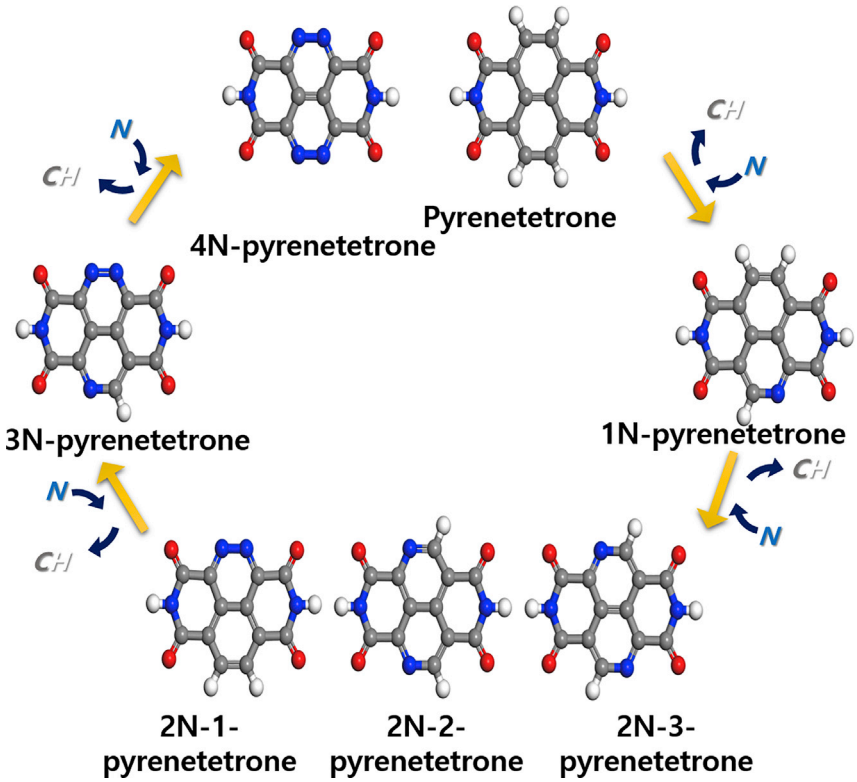

Figure 1. Chemical Structures of Seven Pyrenetetrone Derivatives

The chemical structures of seven pyrenetetrone derivatives, namely, 2,7-di-N-pyrene-1,3,6,8-tetrone (pyrenetetrone), 2,4,7-tri-N-pyrene-1,3,6,8-tetrone (1N-pyrenetetrone), 2,4,5,7-tetra-N-pyrene-1,3,6,8-tetrone (2N-1-pyrenetetrone), 2,4,7,10-tetra-N-pyrene-1,3,6,8-tetrone (2N-2-pyrenetetrone), 2,4,7,9-tetra-N-pyrene-1,3,6,8-tetrone (2N-3-pyrenetetrone), 2,4,5,7,9-penta-N-pyrene-1,3,6,8-tetrone (3N-pyrenetetrone), and 2,4,5,7,9,10-hexa-N-pyrene-1,3,6,8-tetrone (4N-pyrenetetrone). The atoms in gray, white, red, and blue depict carbon, hydrogen, oxygen, and nitrogen, respectively.

stable positions in each pyrenetetrone derivative during the discharging process. This indicates that the *n*th ($n > 1$) Li atom would bind to each pyrenetetrone derivative in which *(n-1)* Li atoms are already bound at their most stable sites. Thus, in the process of identifying the most stable binding configuration for the *n*th Li atom, we do not need to re-examine the most stable configurations for the already bound *(n-1)* Li atoms. In this study, we employed the structural model of each pyrenetetrone derivative with the *(n-1)* Li atoms already bound at their most stable sites to add the *n*th Li atom, considering all possible binding configurations (see Figure S2 for an example of all possible configurations for the first and second Li atoms binding to 4N-pyrenetetrone). The most stable binding configuration for the *n*th Li atom could be identified through this approach.

As shown in Figure S1, Li ions tend to be stored in highly electron-rich places between carbonyl oxygen and nitrogen dopant atoms. Figure 2 shows the change in the redox potential as the number of bound Li atoms increases. The aforementioned redox potentials for the bare molecules at fully charged states are reduced as the number of bound Li atoms increases during the discharging process. For example, the pyrenetetrone having the open circuit voltage of 2.67 V versus Li/Li^+ is predicted to show the redox potentials of 1.54 and −0.28 V versus Li/Li^+ after binding with one and two Li atom(s), respectively. Note that a cathode molecule with a negative value in the redox potential would be no longer reductive, indicating the loss of its cathodic activity. The theoretical Li-storage capability for the pyrenetetrone therefore corresponds to two Li atoms per molecule. Likewise, the other six pyrenetetrone derivatives show quite similar observations on the correlation between the redox potential and the number of bound Li atoms. The redox potentials for the six pyrenetetrone derivatives gradually decrease with the number of bound Li atoms during the discharging process, resulting in the loss of their cathodic activities after binding with certain numbers of Li atoms. Please note that so long as a complex of a

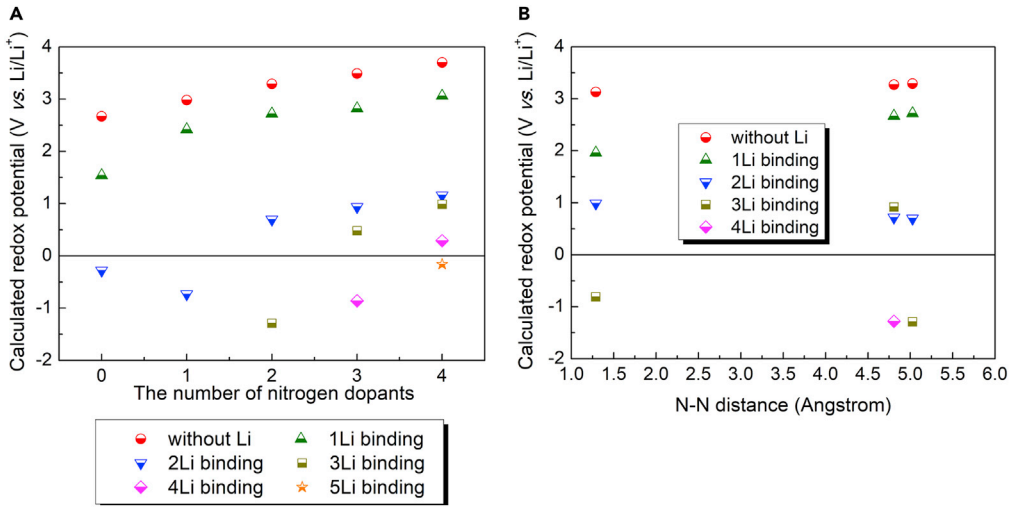

Figure 2. Structure-Dependent Redox Potential during the Discharging Process

(A) The calculated redox potentials for the five pyrenetetrone derivatives, namely, pyrenetetrone, 1N-pyrenetetrone, 2N-3-pyrenetetrone, 3N-pyrenetetrone, and 4N-pyrenetetrone, as a function of the number of incorporated nitrogen dopants during the discharging process.

(B) The redox potentials for the three isomers with two nitrogen dopants, namely, 2N-1-pyrenetetrone, 2N-2-pyrenetetrone, and 2N-3-pyrenetetrone, as a function of the distance between two nitrogen dopants during the discharging process. In (A), 2N-1-pyrenetetrone and 2N-2-pyrenetetrone are not displayed for clarity.

pyrenetetrone derivative without or with bound Li atom(s) is cathodically active, further Li binding of the reduced state of the complex would be thermodynamically favorable as shown in Table S2. In general, the maximum number of Li atoms that can be stored into a pyrenetetrone derivative increases with the number of incorporated nitrogen dopants. This indicates that the addition of a nitrogen dopant would be beneficial to the improvement of the theoretical Li-storage capability. For instance, the three isomers with two nitrogen dopants are predicted to store three to four Li atoms per molecule depending on the geometric configurations of the nitrogen dopants, whereas pyrenetetrone with one nitrogen dopant can store only two Li atoms per molecule. Notably, 4N-pyrenetetrone shows the highest theoretical performance (5 Li atoms per molecule). This is remarkable in comparison with previous computational studies claiming that the maximum number of Li atoms stored into an organic molecule with carbonyl functionality would be equal to or less than the number of the carbonyl groups (Liu et al., 2017; Kim et al., 2016a, 2016b). This suggests that the electron-withdrawing nitrogen dopants and carbonyls would cooperatively strengthen the electron-deficiency in the backbone of the 4N-pyrenetetrone. The relatively densely concentrated electrons near nitrogen dopants are clearly shown in electrostatic potential maps (see Figure 3).

The Li-storage capability discussed earlier can be further quantified in terms of the theoretical charge capacity and energy density to critically assess the performances of the pyrenetetrone derivatives for cathodes in lithium-ion batteries. Figure 4 shows the profiles of the performance parameters during the Li-involved discharging process. Figure S3 describes the electrochemical Li-storage mechanism of 4N-pyrenetetrone during the discharging process, along with its charge capacity profile. Note that the molecular weight of the pyrenetetrone is not significantly changed by the incorporation of nitrogen dopant(s). Thus, a molecule having a higher number of bound Li atoms would show a higher specific charge capacity. As shown in Figure 4, the seven pyrenetetrone derivatives are predicted to have the specific charge capacities of 201–496 mAh/g and the specific energy densities of 424–913 mWh/g. Strikingly, 4N-pyrenetetrone, which can store up to five Li atoms, exhibits the remarkably high performance (496 mAh/g and 913 mWh/g) with five different plateaus in the profiles, outperforming conventional inorganic cathode materials ($LiCoO_2$: 274 mAh/g; $LiFePO_4$: 162 mAh/g and 90–110 mWh/g; $Li[Ni_xCo_yMn_{1-x-y}]O_2$ ($x > 0.9$): 220 mAh/g; $Fe_{0.9}Co_{0.1}OF$ nanorods: 420 mAh/g and ~1000 mWh/g) (Qian et al., 2018; Yamada et al., 2001; Kim et al., 2018; Fan et al., 2018) and other insoluble high-performance organic cathode materials (quinone-based polymers: ~396 mAh/g; poly(benzoquinonyl sulfide: 734 mWh/g) (Wu et al., 2017; Song et al., 2015a, 2015b).

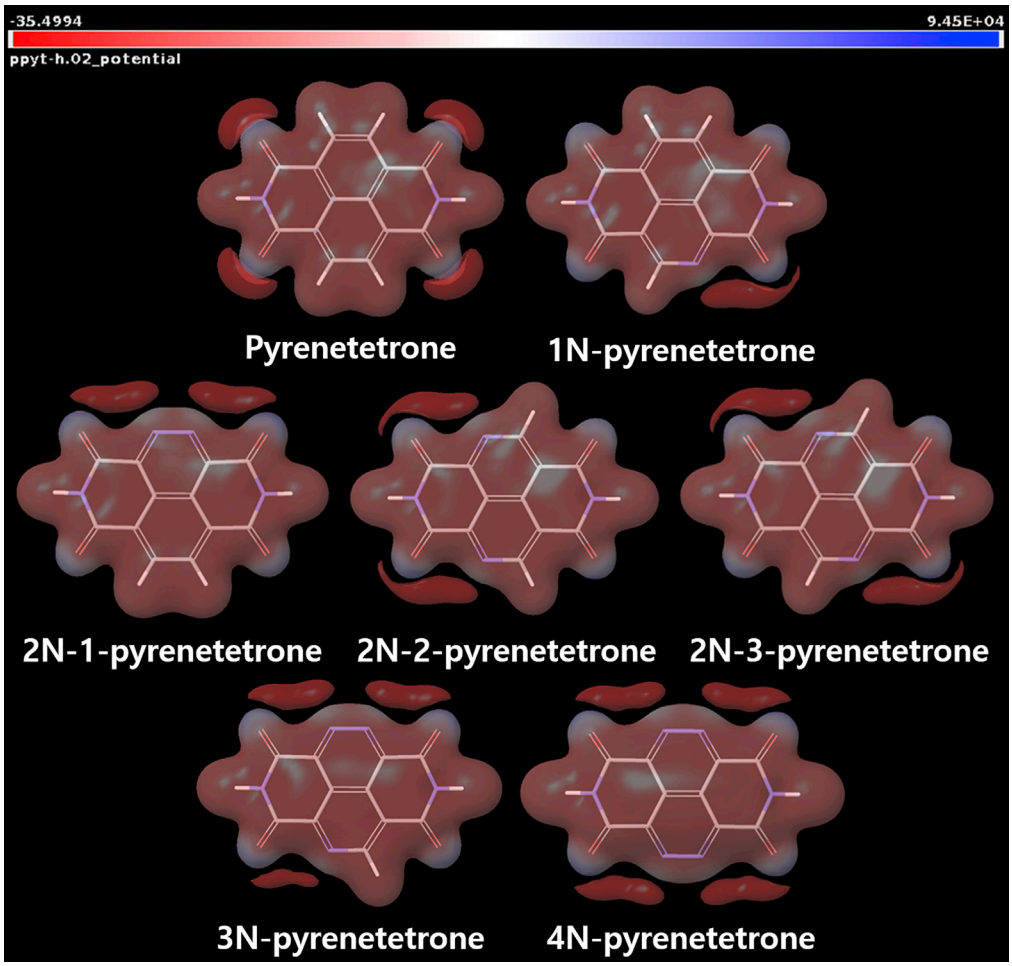

Figure 3. Electrostatic Potential Maps

Visualization of the electrostatic potentials of the seven pyrenetetrone derivatives. Area with more negative electrostatic potential (redder in color) would accept a positive charge more favorably, indicating higher electron density in the area.

It is worthwhile to note that 2N-2-pyrenetetrone storing up to four Li atoms per molecule exhibits the best performance among the three isomers with two nitrogen dopants. However, as shown in Figure 5, the Boltzmann factor-based thermodynamic probability (22.0% in vacuum and 25.3% in solution phase) for the 2N-2-pyrenetetrone is lower than that (76.8% for gas phase and 74.5% for solution phase) for the 2N-3-pyreneteterone, indicating a poor correlation of the performance with the thermodynamic stability (see Figure 4). Considering the thermodynamic probabilities of the three isomers with their performance parameters together, the probability-weighted average charge capacity (energy density) for the three isomers would be predicted to be 322 mAh/g (689 mWh/g) in vacuum and 325 mAh/g (693 mWh/g) in solution phase. It can be concluded from all these observations that the performance parameters would rely on the number of incorporated nitrogen dopants, exhibiting the following order: pyrenetetrone ~ 1N-pyrenetetrone < probability-averaged 2N-pyrenetetrone < 3N-pyrenetetrone < 4N-pyrenetetrone.

Electronic Properties and Solvation Energy

To further understand the redox potentials and theoretical performances of the seven pyrenetetrone derivatives, we investigated their electronic properties, such as electron affinity, the highest occupied molecular orbital (HOMO), and the lowest unoccupied molecular orbital (LUMO). Note that electron affinity is defined by the change in the Gibbs free energy for the reduction of a molecule. Figures 6 and S4 show the correlations of the redox potential with the electronic properties. As expected, the redox potential shows strong correlations with electron affinity, LUMO, and HOMO within the range of positive redox potentials (Méndez-Hernández et al., 2013; Conradie, 2015). It is worthwhile to note that the strong correlations of

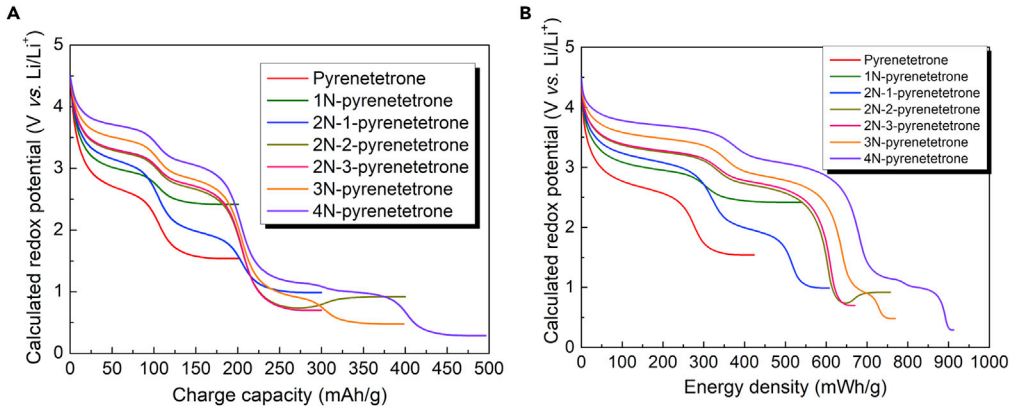

Figure 4. Performance Parameters

Profiles of (A) the charge capacities and (B) the energy densities as a function of the calculated redox potential for seven pyrenetetrone derivatives.

the redox potential with LUMO and HOMO would not guarantee a meaningful correlation between the redox potential and HOMO-LUMO gap. In this study, the linearity for the correlation between the redox potential and LUMO is similar to that for the correlation between the redox potential and HOMO, leading to the HOMO-LUMO gap (2.2–4.0 eV) insensitive to the redox potential. It is unambiguous to conclude that redox-active molecules with more negative values in electron affinity, LUMO, and HOMO would have higher redox potentials due to their enhanced reductive nature. Similar observations have been reported from previous studies on the redox properties of various organic molecules, such as quinones, dopamines, and carbon materials (Liu et al., 2015, 2017; Kim et al., 2016a, 2016b; Zhu et al., 2018; Kang et al., 2018; Park et al., 2017). It is also worthwhile to note that such strong correlations between the redox potential and the electronic properties are limited to the range of positive redox potentials. This indicates that the redox potential would depend not only on the electronic properties but also on other properties, including solvation energy, at the range of negative redox potentials.

To unveil the resources of the poor correlation between redox potential and electron affinity at the range of negative redox potentials, we explored solvation energy as well as electron affinity for each pyrenetetrone derivative. Solvation energy ($\Delta\Delta G^{solv}$) is defined as the change in the solvation free energy during the reduction of a structural model of our interest and can be calculated by "$\Delta\Delta G^{solv} = \Delta G^{solv}(R^-) - \Delta G^{solv}(R)$." Figure S5 shows the collaborative contributions of electron affinity and solvation energy to redox potential for the seven pyrenetetrone derivatives without or with bound Li atoms. Unambiguously, electron affinity would tend to be less negative as the number of bound Li atoms increases during the

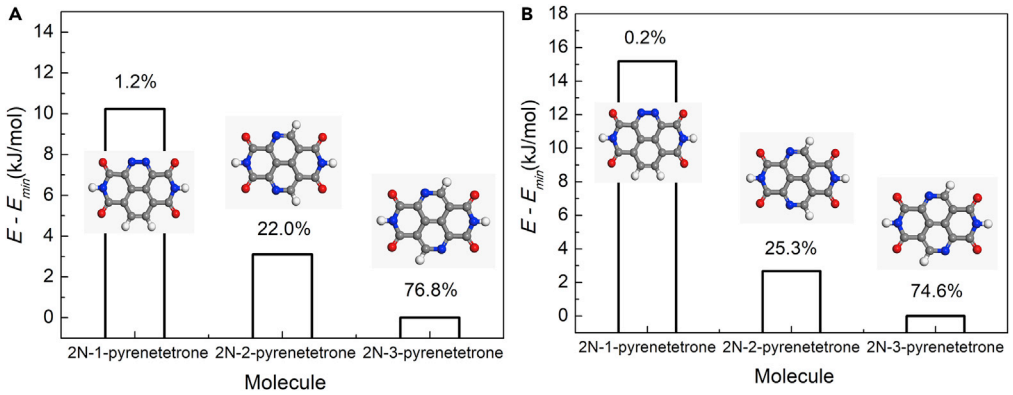

Figure 5. Thermodynamic Stability of Three Isomers

Boltzmann factor-based thermodynamic probabilities for the three isomers with two nitrogen dopants, namely, 2N-1-pyrenetetrone, 2N-2-pyrenetetrone, and 2N-3-pyrenetetrone. In the figure, E_{min} means the Gibbs free energy for the most stable molecule, namely, 2N-3-pyrenentetrone, (A) in vacuum and (B) in solution phase.

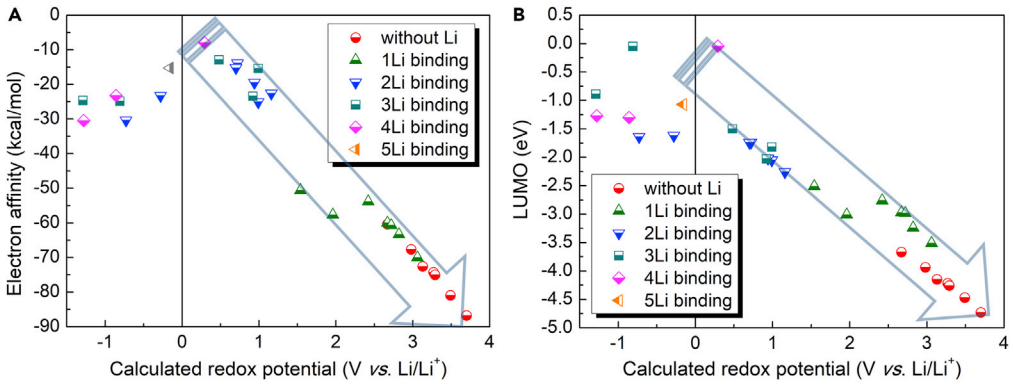

Figure 6. Redox Potential versus Electronic Properties

Correlations of redox potential with (A) electron affinity and (B) LUMO for the seven pyrenetetrone derivatives without or with bound Li atom(s).

discharging process, owing to the decrease in the reductive nature. The organic molecules would become cathodically deactivated, exhibiting negative redox potentials, owing to significant changes in solvation energy. For example, the redox potential of 1N-pyrenetetrone becomes negative and thereby the molecule would lose its cathodic activity after binding with two Li atoms. In this event, its solvation energy significantly changes from negative to positive values. Furthermore, Figure S6 shows a perfect correlation of redox potential with the sum of electron affinity and solvation energy at the range of negative redox potentials. All these imply that solvation energy would be one crucial factor to supplement the poor correlation at the range of negative redox potentials.

The aforementioned collaborative contributions of electron affinity and solvation energy to the redox properties of pyrenetetrone derivatives during the discharging process can be further discussed by an established universal correlation, as shown in Figure 7. The universal correlation of the three key parameters, namely, redox potential, electron affinity, and solvation energy, which is developed using Equation 1 in Supplemental Information with the aim of comprehensively understanding the redox properties for organic materials of our interests, is defined by:

$$y = -nF(z + 1.39) - x = -23.061(z + 1.39) - x \qquad \text{(Equation 1)}$$

Here, x, y, z, n, and F denote electron affinity in kcal/mol, solvation energy in kcal/mol, redox potential in V versus Li/Li^+, the number of electrons transferred, and Faraday constant, respectively. A dotted line is employed in Figure 7A to clarify the correlation ($x + y = -32$) between electron affinity and solvation energy at zero potential. This robust correlation enables us to reliably predict not only the sign (Figure 7A) of the redox potential for an unknown organic compound but also its specific value (Figure 7B) in an efficient manner if electron affinity and solvation energy of the compound are informed. In particular, Figure 7A defines the upper bounds of electron affinity and solvation energy of an organic compound required for sustaining a positive redox potential. For example, an organic compound with electron affinity of −5 kcal/mol would have to sustain its solvation energy below −27 kcal/mol to have a positive redox potential. The most striking feature from the figures is that pyrenetetrone derivatives follow ***two-stage transition behavior*** during the discharging process. Specifically, the redox potentials of pyrenetetrone derivatives are predicted to decrease with the number of bound Li atoms during the discharging process primarily owing to the increase in electron affinity. The cathodic deactivation (i.e., negative redox potential) of the compounds is, however, completed by the critical increase of solvation energy toward positive values. This two-stage transition behavior (see Figures S7 and S8 for clarity) indicates that sustaining solvation energy at negative values during the discharging process would be the crucial factor to improve the theoretical performances of the cathode materials.

DISCUSSION

In this study, we investigated the adequacy of pyrenetetrone and its derivatives as organic cathode materials in lithium-ion batteries. A comprehensive set of seven pyrenetetrone derivatives was prepared by incorporating electron-withdrawing nitrogen dopant(s) into the pristine pyrenetetrone molecule. The first-principles DFT modeling approach was employed to systematically study the electrochemical redox

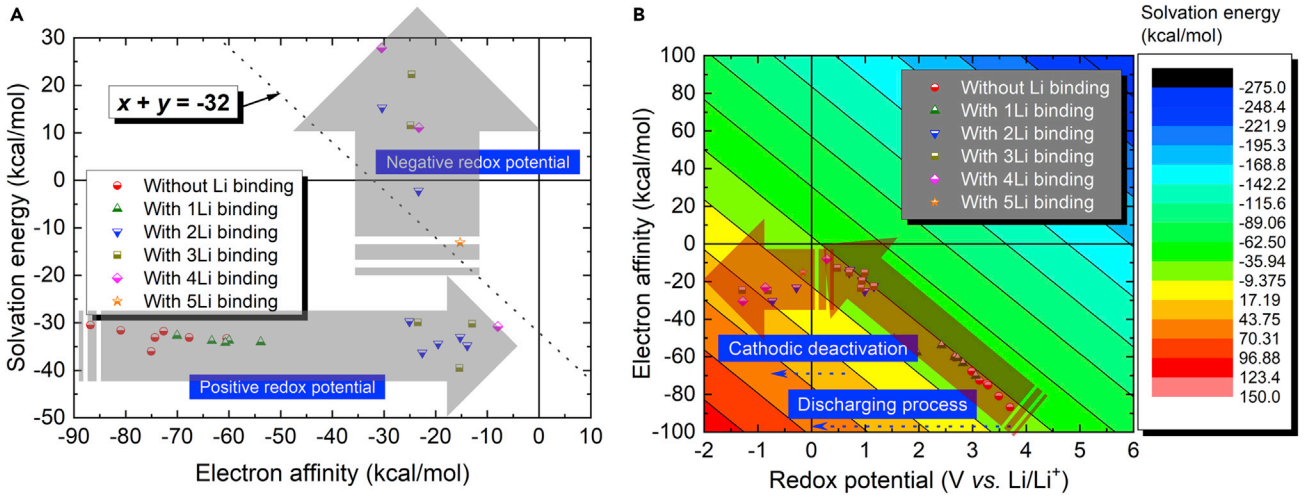

Figure 7. Correlations of Redox Potential–Electron Affinity–Solvation Energy

Correlations between electron affinity and solvation energy for the pyrenetetrone derivatives without and with bound Li atom(s). Correlations to (A) determine the sign of the redox potential and (B) predict a specific redox potential within the range of −2 to 6 V versus Li/Li^+. The shaded arrows describe the two-stage transition behaviors of electron affinity and solvation energy as the redox potential decreases during the discharging process.

properties and performances for the organic molecules. This investigation not only was limited to the bare molecules corresponding to fully charged open-circuit states but also covered the molecules with varied numbers of bound Li atoms to describe the discharging process. The redox properties of the pyrenetetrone derivatives can be summarized by the following features. (1) At the fully charged state, the redox potential increases as the number of electron-withdrawing nitrogen dopants increases, owing to the increase in the electron deficiency of the backbone. (2) At the fully charged state, the redox potential is insensitive to the configuration of doped nitrogen atoms, exhibiting the constant redox potential for three pyrenetetrone derivatives with two nitrogen dopants. (3) The redox potential continuously decreases with the increase in the number of bound Li atoms during the discharging process. The redox potential of each pyrenetetrone derivative becomes negative losing its cathodic activity after binding with a certain number of Li atoms. Notably, 4N-pyrenetetrone loses its cathodic activity exhibiting a negative redox potential after the binding of 5 Li atoms, indicating the Li-storage capability of 5 Li atoms per molecule. This is somewhat surprising since this does not follow a general consensus: the maximum number of Li atoms stored into an organic molecule with carbonyl functionality would be equal to or less than the number of the carbonyl groups in the molecule. This surprising Li-storage capability leads to the remarkably high performance (496 mAh/g and 913 mWh/g). (4) The redox potential is strongly correlated not only with the electronic properties but also with solvation energy, which is a crucial contributor to explain the redox potential at the range of negative values. An established universal correlation verifies that the pyrenetetrone derivatives would exhibit two-stage transition behaviors during the discharging process, highlighting the key contribution of solvation energy to their cathodic deactivation. In conclusion, we believe that the comprehensive understanding of the electrochemical properties for the pyrenetetrone and its nitrogen-doped derivatives would assist us to provide useful information in systematically designing nitrogen-doped organic cathode materials for lithium-ion batteries.

Limitations of the Study

In this article, we investigated the redox properties for a selected set of nitrogen-doped pyrenetetrone derivatives and their theoretical performances to assess their potential for organic cathodes in lithium-ion batteries. This enabled us to systematically study these thermodynamic characteristics with the aim of suggesting guidelines for a desired design strategy of pyrenetetrone-based organic cathode materials. However, despite these efforts, the understanding on the ionic diffusivities and electronic conductivities of the organic compounds is still lacking and needs to be explored. In future work, we plan to comprehensively study the kinetic characteristics of the organic compounds.

METHODS

All methods can be found in the accompanying Transparent Methods supplemental file.

SUPPLEMENTAL INFORMATION

Supplemental Information can be found online at https://doi.org/10.1016/j.isci.2019.10.023.

ACKNOWLEDGMENTS

This work was supported by the National Research Foundation of Korea (NRF) funded by the Ministry of Science, ICT & Future Planning (NRF-2017R1C1B5017482).

AUTHOR CONTRIBUTIONS

All authors have given approval to the final version of the manuscript. The manuscript was written through contributions of all authors.

DECLARATION OF INTERESTS

There are no conflicts of interest to declare.

Received: September 4, 2019
Revised: October 1, 2019
Accepted: October 11, 2019
Published: November 22, 2019

REFERENCES

Araujo, R.B., Banerjee, A., Panigrahi, P., Strømme, L.Y.M., Sjodin, M., Araujo, C.M., and Ahuja, R. (2017). Designing strategies to tune reduction potential of organic molecules for sustainable high capacity battery application. J. Mater. Chem. A *5*, 4430–4454.

Aurbach, D., Talyosef, Y., Markovsky, B., Markevich, E., Zinigrad, E., Asraf, L., Gnanaraj, J.S., and Kim, H.-J. (2004). Design of electrolyte solutions for Li and Li-ion batteries: a review. Electrochim. Acta *50*, 247–254.

Chen, H., Cong, T.N., Yang, W., Tan, C., Li, Y., and Ding, Y. (2009). Progress in electrical energy storage system: a critical review. Prog. Nat. Sci. *19*, 291–312.

Conradie, J. (2015). A Frontier orbital energy approach to redox potentials. J. Phys. Conf. Ser. *633*, 012045.

Dincer, I. (2000). Renewable energy and sustainable development: a crucial review. Renew. Sustain. Energ. Rev. *4*, 157–175.

Er, S., Suh, C., Marshak, M.P., and Aspuru-Guzik, A. (2015). Computational design of molecules for an all-quinone redox flow battery. Chem. Sci. *6*, 885–893.

Fan, X., Hu, E., Ji, X., Zhu, Y., Han, F., Hwang, S., Liu, J., Bak, S., Ma, Z., Gao, T., et al. (2018). High energy-density and reversibility of iron fluoride cathode enabled via an intercalation extrusion reaction. Nat. Commun. *9*, 2324.

Goodenough, J.B., and Park, K.S. (2013). The Li-ion rechargeable battery: a perspective. J. Am. Chem. Soc. *135*, 1167–1176.

Gür, T.M. (2018). Review of electrical energy storage technologies, materials and systems: challenges and prospects for large-scale grid storage. Energy Environ. Sci. *11*, 2696–2767.

Herbert, G.M.J., Iniyan, S., Sreevalsan, E., and Rajapandian, S. (2007). A review of wind energy technologies. Renew. Sustain. Energ. Rev. *11*, 1117–1145.

Kang, J., Kim, K.C., and Jang, S.S. (2018). Density functional theory modeling-assisted investigation of thermodynamics and redox properties of boron-doped corannulenes for cathodes in lithium-ion batteries. J. Phys. Chem. C *122*, 10675–10681.

Kim, S., Kim, K.C., Lee, S.W., and Jang, S.S. (2016a). Thermodynamic and redox properties of graphene oxides for Lithium-Ion battery applications: first principles density functional theory modeling approach. Phys. Chem. Chem. Phys. *18*, 20600–20606.

Kim, K.C., Liu, T., Lee, S.W., and Jang, S.S. (2016b). First-principles density functional theory modeling of Li binding: thermodynamics and redox properties of quinone derivatives for lithium-ion batteries. J. Am. Chem. Soc. *138*, 2374–2382.

Kim, U.-H., Jun, D.-W., Park, K.-J., Zhang, Q., Kaghazchi, P., Aurbach, D., Major, D.T., Goobes, G., Dixit, M., Leifer, N., et al. (2018). Pushing the limit of layered transition metal oxide cathodes for high-energy density rechargeable Li ion batteries. Energy Environ. Sci. *11*, 1271–1279.

Lee, S.W., Yabuuchi, N., Gallant, B.M., Chen, S., Kim, B.-S., Hammond, P.T., and Shao-Horn, Y. (2010). High-power lithium batteries from functionalized carbon-nanotube electrodes. Nat. Nanotechnol. *5*, 531–537.

Lee, S.W., Gallant, B.M., Byon, H.R., Hammond, P.T., and Shao-Horn, Y. (2011). Nanostructured carbon-based electrodes: bridging the gap between thin-film lithium-ion batteries and electrochemical capacitors. Energy Environ. Sci. *4*, 1972–1985.

Liu, T., Kim, K.C., Kavian, R., Jang, S.S., and Lee, S.W. (2015). High-density Lithium-Ion energy storage utilizing the surface redox reactions in folded graphene films. Chem. Mater. *27*, 3291–3298.

Liu, T., Kim, K.C., Lee, B., Chen, Z., Noda, S., Jang, S.S., and Lee, S.W. (2017). Self-polymerized dopamine as an organic cathode for Li- and Na ion batteries. Energy Environ. Sci. *10*, 205–215.

Lund, J.W., and Boyd, T.L. (2016). Direct utilization of geothermal energy 2015 worldwide review. Geothermics *60*, 66–93.

Luo, Z., Liu, L., Ning, J., Lei, K., Lu, Y., Li, F., and Chen, J. (2018). A microporous covalent–organic framework with abundant accessible carbonyl groups for lithium-ion batteries. Angew. Chem. Int. Ed. *57*, 9443–9446.

Ma, T., Zhao, Q., Wang, J., Pan, Z., and Chen, J. (2016). A sulfur heterocyclic quinone cathode and a multifunctional binder for a high-performance rechargeable lithium-ion battery. Angew. Chem. Int. Ed. *55*, 6428–6432.

Marom, R., Amalraj, S.F., Leifer, N., Jacob, D., and Aurbach, D. (2011). A review of advanced and practical lithium battery materials. J. Mater. Chem. *21*, 9938–9954.

Méndez-Hernández, D.D., Tarakeshwar, P., Gust, D., Moore, T.A., Moore, A.L., and Mujica, V. (2013). Simple and accurate correlation of experimental redox potentials and

DFT-calculated HOMO/LUMO energies of polycyclic aromatic hydrocarbons. J. Mol. Model. *19*, 2845–2848.

Meng, Y.S., and Dompablo, M.E. (2009). First principles computational materials design for energy storage materials in lithium ion batteries. Energy Environ. Sci. *2*, 589–609.

Nitta, N., Wu, F., Lee, J.T., and Yushin, G. (2015). Li-ion battery materials: present and future. Mater. Today *18*, 252–264.

Nokami, T., Matsuo, T., Inatomi, Y., Hojo, N., Tsukagoshi, T., Yoshizawa, H., Shimizu, A., Kuramoto, H., Komae, K., Tsuyama, H., and Yoshida, J.-I. (2012). Polymer-bound pyrene-4,5,9,10-tetraone for fast-charge and -discharge lithium-ion batteries with high capacity. J. Am. Chem. Soc. *134*, 19694–19700.

Ong, S.P., Chevrier, V.L., Hautier, G., Jain, A., Moore, C., Kim, S., Ma, X., and Ceder, G. (2011). Voltage, stability and diffusion barrier differences between sodium-ion and lithium-ion intercalation materials. Energy Environ. Sci. *4*, 3680–3688.

Park, J.H., Liu, T., Kim, K.C., Lee, S.W., and Jang, S.S. (2017). Systematic moleecular design of Ketone derivatives of aromatic molecules for Lithium ion batteries: first-principles DFT modeling. ChemSusChem *10*, 1584–1591.

Qian, J., Liu, L., Yang, J., Li, S., Wang, X., Zhuang, H.L., and Lu, Y. (2018). Electrochemical surface passivation of LiCoO2 particles at ultrahigh voltage and its applications in lithium-based batteries. Nat. Commun. *9*, 4918.

Roth, H.G., Romero, N.A., and Nicewicz, D.A. (2016). Experimental and calculated electrochemical potentials of common organic molecules for applications to single-electron redox chemistry. Synlett *27*, 714–723.

Schon, T.B., Tilley, A.J., Bridges, C.R., Miltenburg, M.B., and Seferos, D.S. (2016). Bio-derived polymers for sustainable lithium-ion batteries. Adv. Funct. Mater. *26*, 6896–6903.

Solangi, K.H., Islam, M.R., Saidur, R., Rahim, N.A., and Fayaz, H. (2011). A review on global solar energy policy. Renew. Sustain. Energ. Rev. *15*, 2149–2163.

Song, Z., Qian, Y., Zhang, T., Otani, M., and Zhou, H. (2015a). Poly(benzoquinonyl sulfide) as a high-energy organic cathode for rechargeable Li and Na batteries. Adv. Sci. *2*, 1500124.

Song, Z., Qian, Y., Gordin, M.L., Tang, D., Xu, T., Otani, M., Zhan, H., Zhou, H., and Wang, D. (2015b). Polyanthraquinone as a reliable organic electrode for stable and fast lithium storage. Angew. Chem. Int. Ed. *54*, 13947–13951.

Takahashi, Y., Tode, S., Kinoshita, A., Fujimoto, H., Nakane, I., and Fujitani, S. (2008). Development of lithium-ion batteries with a LiCoO2 cathode toward high capacity by elevating charging potential. J. Electrochem. Soc. *155*, A537–A541.

Wang, D.-W., Sun, C., Zhou, G., Li, F., Wen, L., Donose, B.C., Lu, G.Q., Cheng, H.-M., and Gentle, I.R. (2013). The examination of graphene oxide for rechargeable lithium storage as a novel cathode material. J. Mater. Chem. A *1*, 3607–3612.

Wu, Y., Zeng, R., Nan, J., Shu, D., Qiu, Y., and Chou, S.L. (2017). Quinone electrode materials for rechargeable lithium/sodium ion batteries. Adv. Energy Mater. *7*, 1700278.

Xiang, Y., Li, J., Lei, J., Liu, D., Xie, Z., Qu, D., Li, K., Deng, T., and Tang, H. (2016). Advanced separators for lithium-ion and lithium–sulfur batteries: a review of recent progress. ChemSusChem *9*, 3023–3039.

Yamada, A., Chung, S.C., and Hinokuma, K. (2001). Optimized LiFePO4 for lithium battery cathodes. J. Electrochem. Soc. *148*, A224–A229.

Zhu, Y., Kim, K.C., and Jang, S.S. (2018). Boron-doped coronenes with high redox potential for organic positive electrodes in lithium-ion batteries: a first-principles density functional theory modeling study. J. Mater. Chem. A *6*, 10111–10120.

ISCI, Volume *21*

Supplemental Information

Pyrenetetrone Derivatives Tailored by Nitrogen Dopants for High-Potential Cathodes in Lithium-Ion Batteries

Chae Young Go, Gyeong Seok Jeong, and Ki Chul Kim

Supplemental Information for

Pyrenetetrone Derivatives Tailored by Nitrogen Dopants for High-Potential Cathodes in Lithium-Ion Batteries

Chae Young Go,[1] Gyeong Seok Jeong[1] and Ki Chul Kim[1,2,*]

[1]Computational Materials Design Laboratory, Division of Chemical Engineering, Konkuk University, Seoul 05029, The Republic of Korea
[2]Lead Contact

*Correspondence: kich2018@konkuk.ac.kr (K. C. Kim)

TRANSPARENT METHODS

All DFT calculations were performed by Jaguar with Perdew-Burke-Ernzehof hybrid (PBE0) functional and 6-31+G(d,p) basis set.(Bochevarov et al., 2013; Adamo et al., 1999; Adamo and Barone, 1999) As shown in Figure 1, a series of seven pyrenetetrone derivatives with varied numbers and positions of nitrogen dopants were structurally modeled and geometrically optimized using the DFT method to study their redox properties. The pyrenetetrone derivatives are shortly named by pyrenetetrone, 1N-pyrenetetrone, 2N-1-pyrenetetrone, 2N-2-pyrenetetrone, 2N-3-pyrenetetrone, 3N-pyrenetetrone, and 4N-pyrenetetrone for 2,7-di-N-pyrene-1,3,6,8-tetrone, 2,4,7-tri-N-pyrene-1,3,6,8-tetrone, 2,4,5,7-tetra-N-pyrene-1,3,6,8-tetrone, 2,4,7,10-tetra-N-pyrene-1,3,6,8-tetrone, 2,4,7,9-tetra-N-pyrene-1,3,6,8-tetrone, 2,4,5,7,9-penta-N-pyrene-1,3,6,8-tetrone, and 2,4,5,7,9,10-hexa-N-pyrene-1,3,6,8-tetrone, respectively.

The thermodynamic cycle described by Truhlar and coworkers was used to compute the redox potentials of the pyrenetetrone derivatives.(Winget et al., 2004; Winget et al., 2000) The redox potential ($\Delta \boldsymbol{E^{red}}$) of an organic cathode material in solution phase with respect to a Li/Li$^+$ reference anode can be defined by

$$\Delta E^{red} = \frac{-\Delta G^{red}(R,soln)}{nF} - 1.39\ V \quad . \tag{1}$$

Here, $\Delta G^{red}(R, soln)$ is the change in the DFT-computed Gibbs free energy in solution phase during the reduction of the cathode material, *R*, at 298.15 K, *n* is the number of electrons transferred during the reduction, and *F* is Faraday constant. The constant, 1.39 V, is introduced to convert the redox potential into the reference Li electrode. Based on the thermodynamic cycle, the change in the Gibbs free energy in solution phase during the reduction of the cathode material would be calculated by

$$\Delta G^{red}(R, soln) = \Delta G^{red}(R, vacuum) + \Delta G^{solv}(R^-) - \Delta G^{solv}(R) \quad . \tag{2}$$

Here, $\Delta G^{red}(R, vacuum)$ is the change in the Gibbs free energy in vacuum during the reduction, $\Delta G^{solv}(R^-)$ is the solvation free energy for the species in the anionic state, and $\Delta G^{solv}(R)$ is the solvation free energy for the species in the neutral state. The solvation free energies were calculated using Poisson-Boltzmann implicit solvation model to consider the contribution of the solvation to the free energy. A dielectric constant of 16.14, which would reliably describe the polarity of the solvents in mixture (ethylene carbonate and dimethyl carbonate (3:7 v/v)), was used to perform the solvation free energy calculations. This approach was employed to examine the redox potentials not only for the pristine molecules but also for the molecules with different numbers of bound Li atoms.

As stated earlier, electron affinity ($EA(R, vacuum)$) is defined by the change in the Gibbs free energy for the reduction of an organic material, R in vacuum, at 298.15 K. The mathematical form of electron affinity is written by

$$EA(R, vacuum) = G(R^-, vacuum) - G(R, vacuum) \quad . \tag{3}$$

Here, $G(R, vacuum)$ and $G(R^-, vacuum)$ are the DFT-computed Gibbs free energies for the material in the neutral and anionic states, in vacuum, respectively. To predict electron affinity of a given organic material, we geometrically optimized the structure of the material followed by the vibrational frequency calculation in each of neutral and anionic states.

Based on the Li-storage capabilities for the organic molecules of our interest, we further calculated their theoretical charge capacities (Q) which could be defined by

$$Q(\frac{mAh}{g}) = \frac{nF}{3.6M_w} \tag{4}$$

where, M_w means the molecular weight. The gravimetric charge capacity is defined by the amount of charge carriers stored into unit mass of a cathode material. It is unambiguous that an organic cathode material with higher gravimetric charge capacity would require less cathode weight for the material to store a targeted amount of charge carriers, leading to the reduction in the battery weight. It is therefore important to identify organic cathode materials with high gravimetric charge capacities. The theoretical energy density (W) of the molecule was also computed by

$$W\ (mWh/g) = \int_0^Q V(q)dq \quad . \tag{5}$$

Here, V is the redox potential with respect to Li electrode.

The thermodynamic probabilities of three pyrenetetrone derivatives with two nitrogen dopants, namely, 2N-1-pyrenetetrone, 2N-2-pyrenetetrone, and 2N-3-pyrenetetrone, would strongly rely on their relative thermodynamic stability which is described by the Boltzmann factor (F_i). Specifically, the Boltzmann factor for each pyrenetetrone derivative was computed by

$$F_i = e^{-\frac{E_i}{k_B T}} \quad . \tag{6}$$

Here, E_i represents the Gibbs free energy of the pyrenetetrone derivative either in vacuum or in solution phase, k_B depicts the Boltzmann constant, and T is temperature (298.15 K). The thermodynamic probability of the pyrenetetrone derivative is computed by its Boltzmann factor averaged by the sum of the Boltzmann factors for all the three pyrenetetrone derivatives.

Table S1. Database for redox properties of organic compounds. Redox potentials for seven pyrenetetrone derivatives, namely 2,7-N-1,3,6,8-pyrenetetrone (pyrenetetrone), 2,4,7-N-1,3,6,8-pyrenetetrone (1N-pyrenetetrone), 2,4,5,7-N-1,3,6,8-pyrenetetrone (2N-1-pyrenetetrone), 2,4,7,10-N-1,3,6,8-pyrenetetrone (2N-2-pyrenetetrone), 2,4,7,9-N-1,3,6,8-pyrenetetrone (2N-3-pyrenetetrone), 2,4,5,7,9-N-1,3,6,8-pyrenetetrone (3N-pyrenetetrone), and 2,4,5,7,9,10-N-1,3,6,8-pyrenetetrone (4N-pyrenetetrone), without or with bound Li atom(s). Related to Figure 2.

Model	Redox potential (V *vs.* Li/Li^+)					
	Without Li	1 Li binding	2 Li binding	3 Li binding	4 Li binding	5 Li binding
Pyrenetetrone	2.67	1.54	-0.28	-	-	-
1N-pyrenetetrone	2.98	2.42	-0.73	-	-	-
2N-1-pyrenetetrone	3.13	1.96	0.99	-0.81	-	-
2N-2-pyrenetetrone	3.27	2.67	0.72	0.92	-1.28	-
2N-3-pyrenetetrone	3.29	2.72	0.7	-1.29	-	-
3N-pyrenetetrone	3.49	2.82	0.94	0.48	-0.86	-
4N-pyrenetetrone	3.7	3.06	1.16	0.99	0.29	-0.16

Table S2. Li binding free energies of organic compounds. Binding free energies of seven pyrenetetrone derivatives with Li both in vacuum and solution phase (corresponding to the solvents in mixture of ethylene carbonate and dimethyl carbonate (3:7 v/v). The *n* Li binding (*n* >1) for a pyrenetetrone derivative represents the binding of the *n*th Li to the pyrenetetrone derivative with already bound *(n-1)* Li atoms. Binding free energy can be defined by the change in the free energy during the binding process. Related to Figures 2 and 3.

Model	Li binding free energy in vacuum (solution phase) (kJ/mol)				
	1 Li binding	2 Li binding	3 Li binding	4 Li binding	5 Li binding
Pyrenetetrone	-148 (-271)	-165 (-150)	-	-	-
1N-pyrenetetrone	-285 (-308)	-173 (-219)	-	-	-
2N-1-pyrenetetrone	-304 (-325)	-255 (-276)	-87 (-94)	-	-
2N-2-pyrenetetrone	-295 (-330)	-300 (-299)	-30 (122)	-25 (-96)	-
2N-3-pyrenetetrone	-294 (-330)	-301 (-302)	-37 (-103)	-	-
3N-pyrenetetrone	-322 (-354)	-296 (-305)	-173 (-151)	-53 (-52)	-
4N-pyrenetetrone	-328 (-369)	-322 (-328)	-177 (-161)	-92 (-68)	-130 (-126)

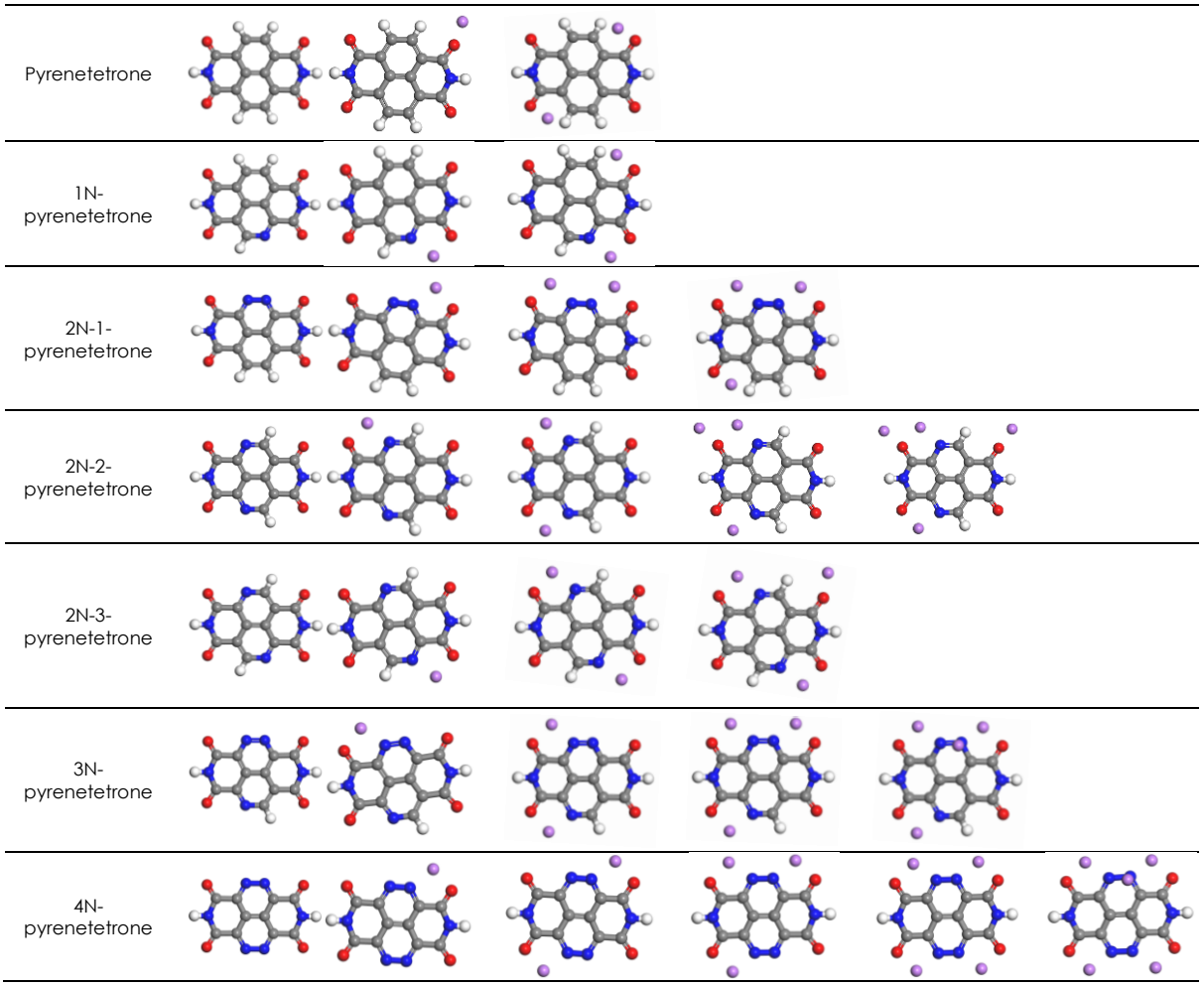

Figure S1. Visualization for the Li-storage processes of pyrenetetrone derivatives. Li-binding mechanisms for seven pyrenetetrone derivatives, namely pyrenetetrone, 1N-pyrenetetrone, 2N-1-pyrenetetrone, 2N-2-pyrenetetrone, 2N-3-pyrenetetrone, 3N-pyrenetetrone, and 4N-pyrenetetrone. Related to Figures 2 and 3.

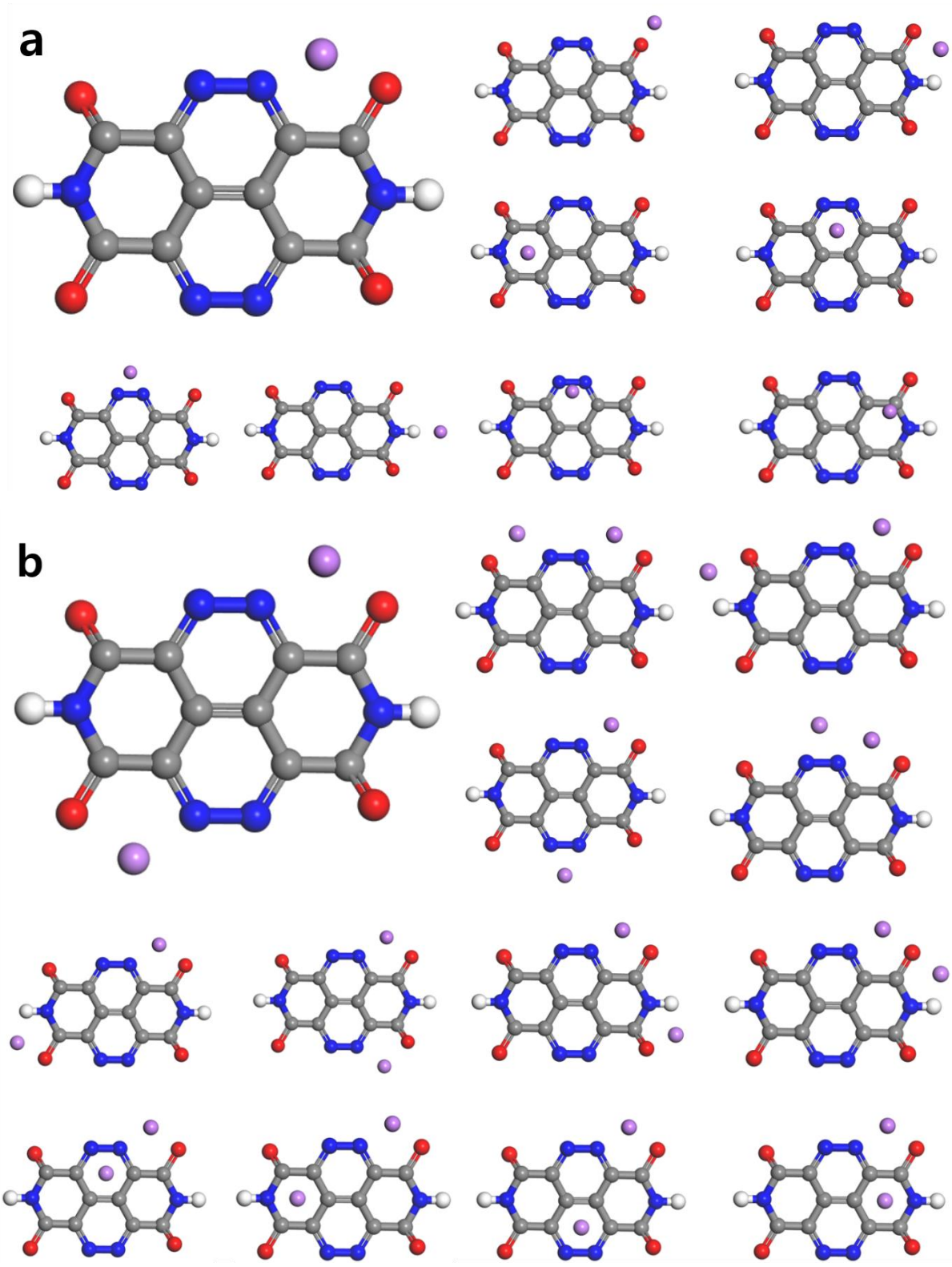

Figure S2. All possible Li-binding configurations. All possible binding configurations for the (a) first and (b) second Li atoms binding to 4N-pyrenetetrone. Related to Figures 2 and 3.

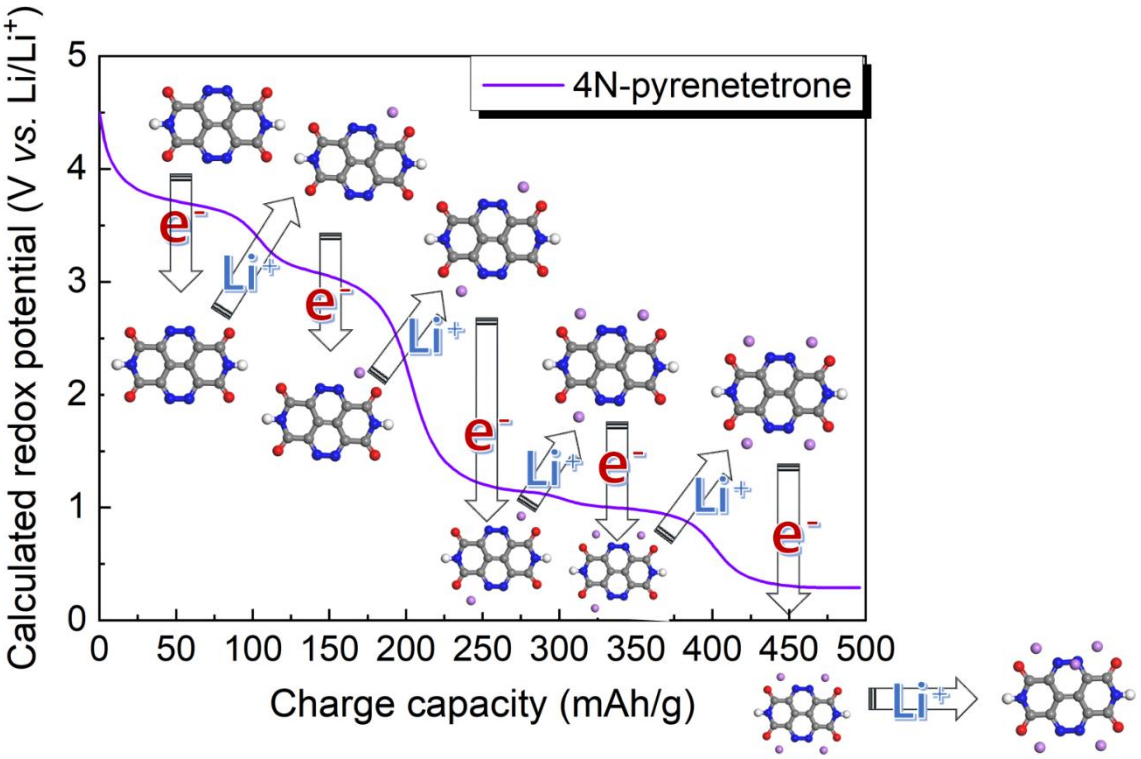

Figure S3. Electrochemical Li-storage mechanism of 4N-pyrenetetrone. Detailed description of the electrochemical Li-storage mechanism for 4N-pyrenetetrone during the discharging process, along with its charge capacity profile. Five Li^+-e^- pairs are predicted to be stored in 4N-pyrenetetrone. Related to Figure 4.

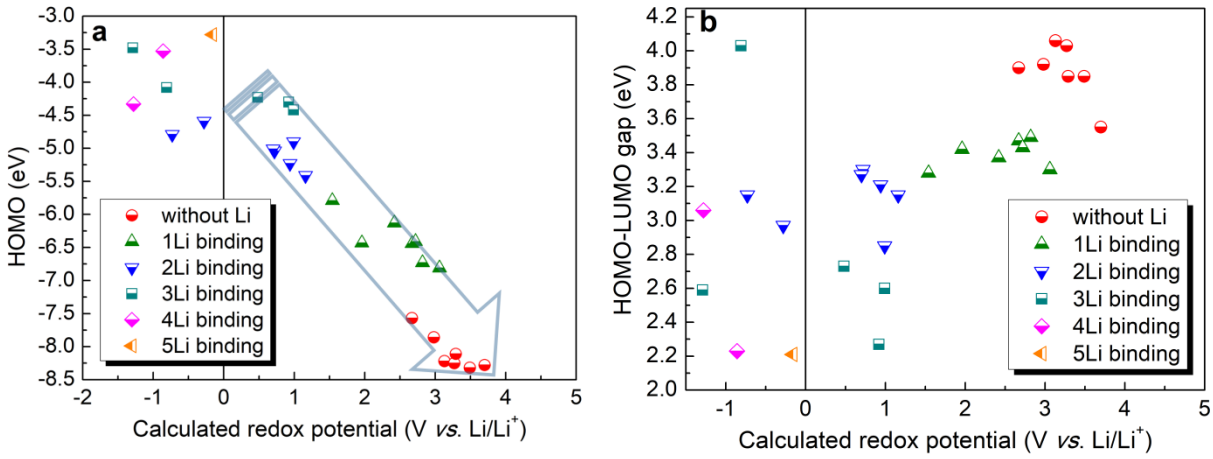

Figure S4. Redox potential *vs.* electronic properties. Correlations of redox potential with (a) HOMO and (b) HOMO-LUMO gap for the seven pyrenetetrone derivatives without or with bound Li atom(s). Related to Figure 6.

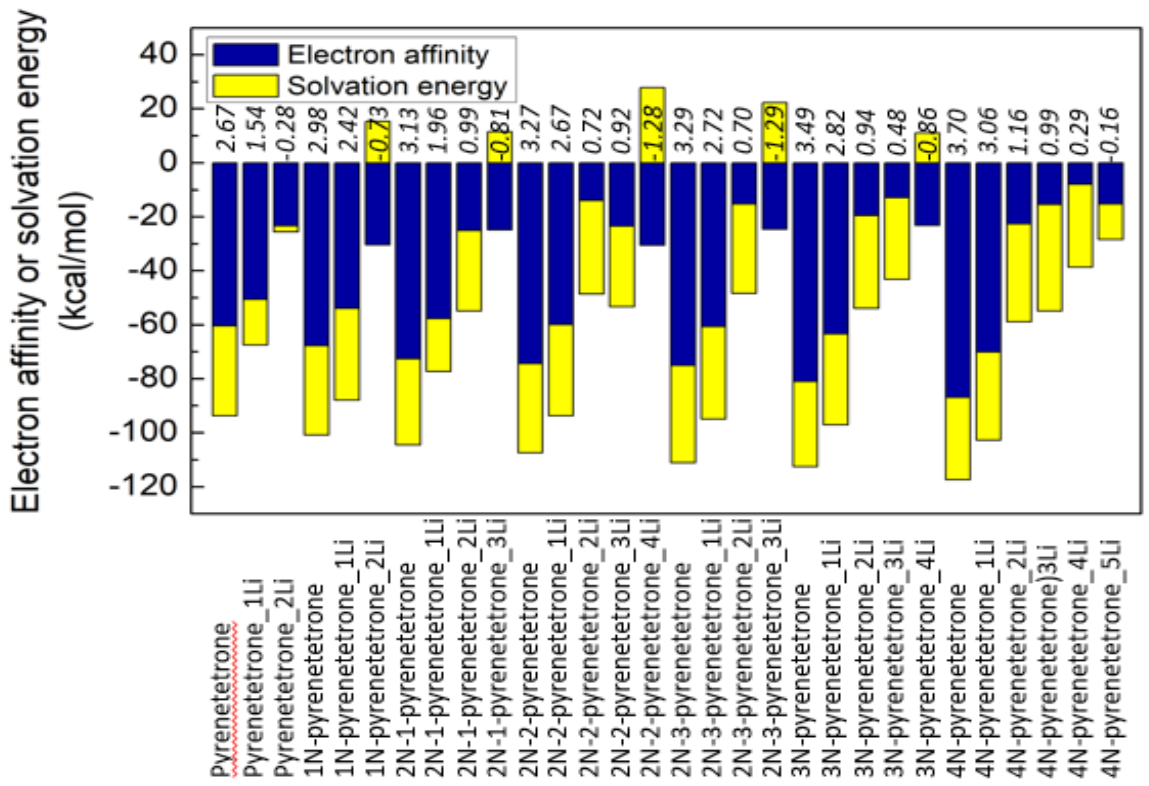

Figure S5. Correlations of redox potential with electron affinity and solvation energy. The contributions of two primary contributors, namely electron affinity and solvation energy, to redox potential for the seven pyrenetetrone derivatives without or with bound Li atom(s). Their redox potentials are depicted in the figure in unit of V *vs.* Li/Li^+. Related to Figure 7.

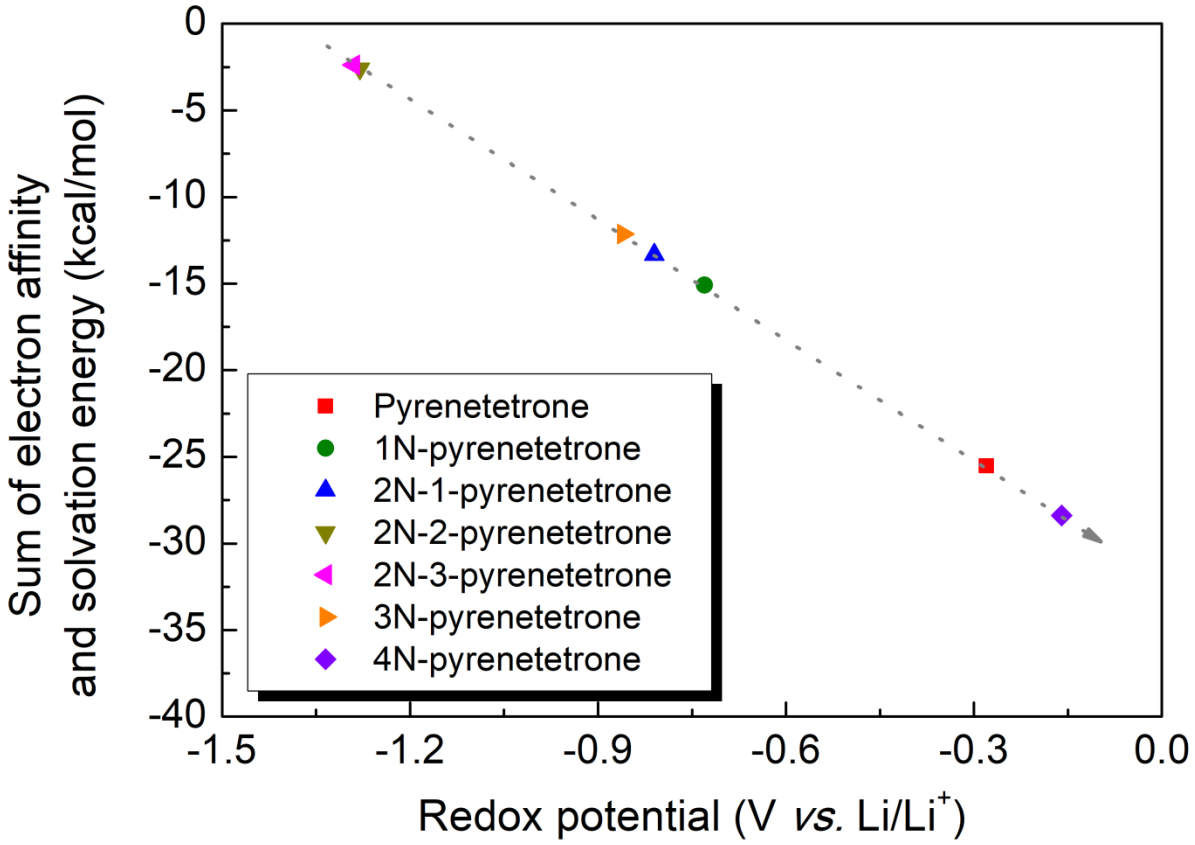

Figure S6. Correlations of redox potential with electron affinity and solvation energy. The correlation of redox potential with the sum of electron affinity and solvation energy for the pyrenetetrone derivatives at the range of negative redox potentials. Related to Figure 7.

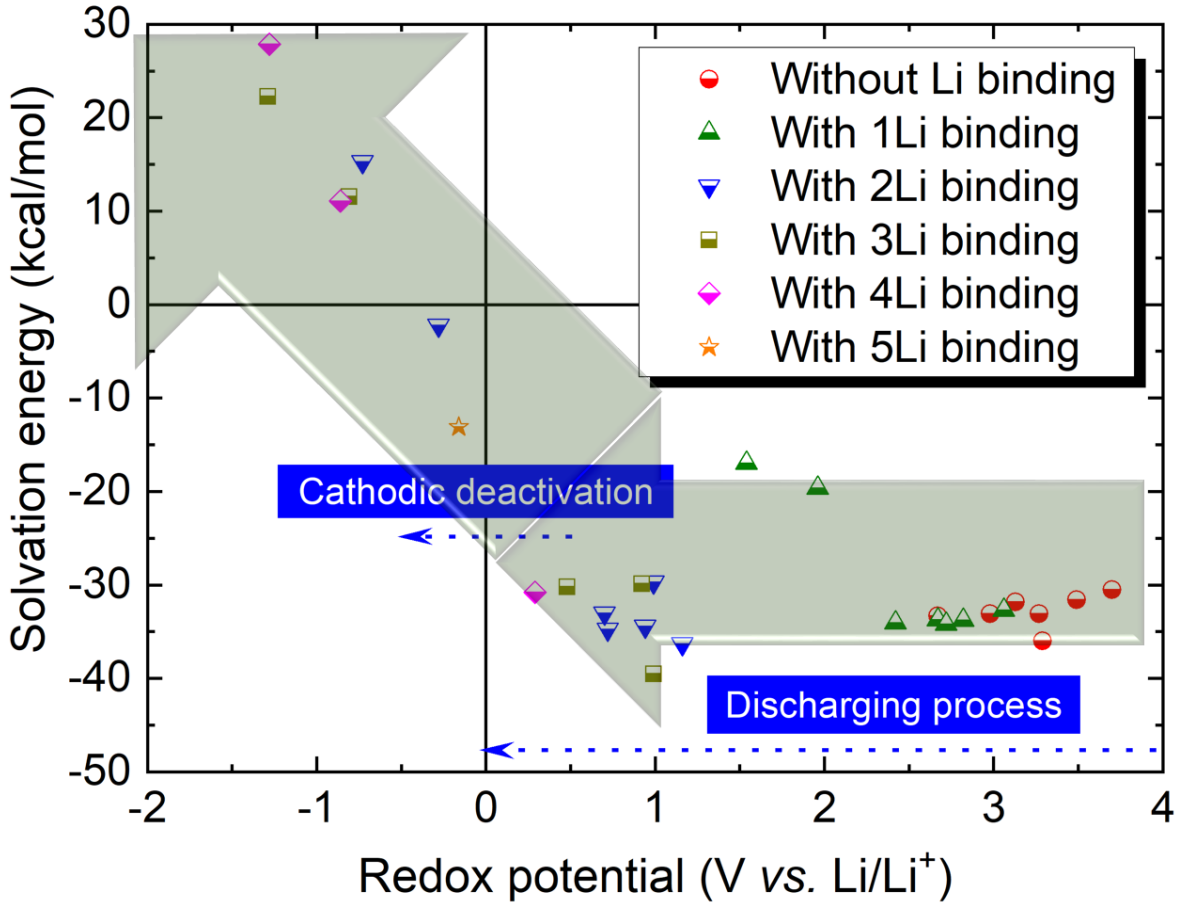

Figure S7. Solvation energy profile. Correlation of redox potential with solvation energy for all the pyrenetetrone derivatives without or with bound Li atom(s). The two big arrows describe the two-stage transition behavior of solvation energy as the redox potential decreases during the discharging process, highlighting the critical role of solvation energy in the cathodic deactivation. Related to Figure 7.

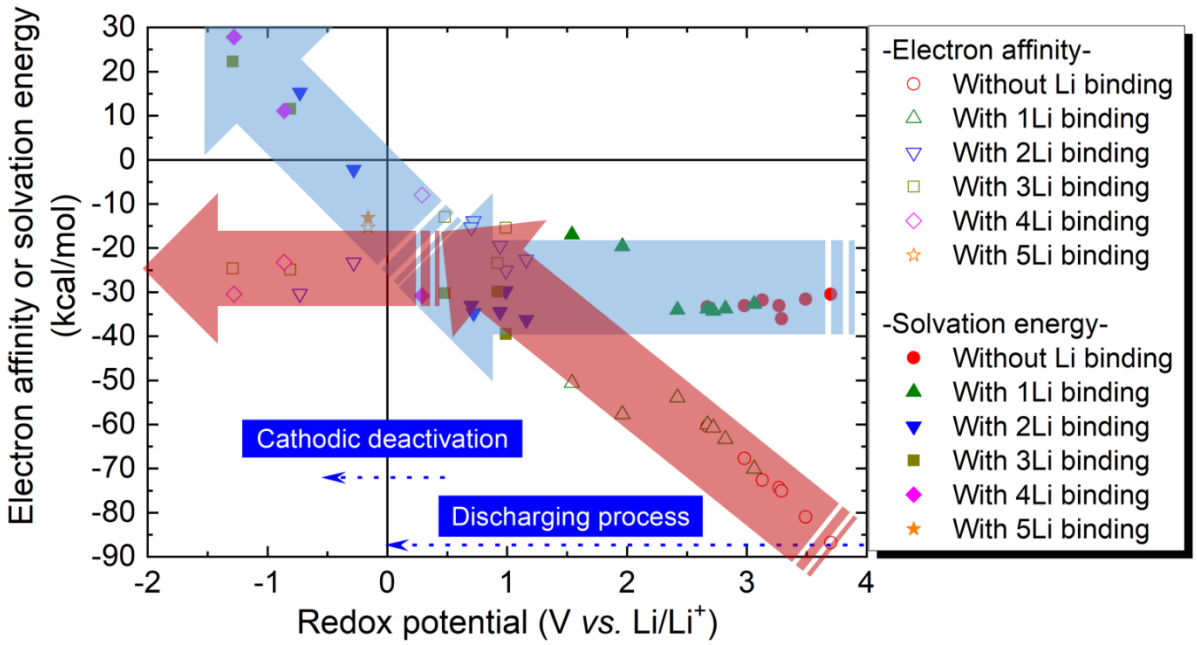

Figure S8. Electron affinity and solvation energy profiles. Correlations of redox potential with electron affinity and solvation energy for all the pyrenetetrone derivatives without or with bound Li atom(s). The big arrows in red (blue) describe the two-stage transition behavior of electron affinity (solvation energy) as the redox potential decreases during the discharging process. This highlights that electron affinity would be the critical factor for the decrease in the redox potential during the discharging process (at the range of positive redox potentials) while the cathodic activity would be deactivated by solvation energy. Related to Figure 7.

REFERENCES

Bochevarov, A.D., Harder, E., Hughes, T.F., Greenwood, J.R., Braden, D.A., Philipp, D.M., Rinaldo, D., Halls, M.D., Zhang, J., and Friesner, R.A. (2013). Jaguar: a high-performance quantum chemistry software program with strengths in life and materials sciences. Int. J. Quantum Chem. *113*, 2110-2142.

Adamo, C., Scuseria, G.E., and Barone, V. (1999). Accurate excitation energies from time-dependent density functional theory: Assessing the PBE0 model. J. Chem. Phys. *111*, 2889-2899.

Adamo, C., and Barone, V. (1999). Toward reliable density functional methods without adjustable parameters: The PBE0 model. J. Chem. Phys. *110*, 6158-6170.

Winget, P., Cramer, C.J., and Truhlar, D.G. (2004). Computation of equilibrium oxidation and reduction potentials for reversible and dissociative electron-transfer reactions in solution. Theor. Chem. Acc. *112*, 217-227.

Winget, P., Weber, E.J., Cramer, C.J., and Truhlar, D.G. (2000). Computational electrochemistry : aqueous one-electron oxidation potentials for substituted anilines. Phys. Chem. Chem. Phys. *2*, 1231-1239.